

Raman microprobe studies of dissolution of microporous faujasitic-like zincophosphate crystals

Mario J. Castagnola, Prabir K. Dutta *

Department of Chemistry, The Ohio State University, 120 W 18th Avenue, Columbus, OH 43210-1185, USA

Received 20 July 2000; accepted 30 October 2000

Abstract

Dissolution of large platelet-like ($\sim 100 \mu\text{m}$) crystals of the faujasitic zincophosphate-X (ZnPO-X) were examined using Raman microprobe spectroscopy in the presence of a series of monovalent ions. Sodium ions did not alter the ZnPO-X framework, whereas in the presence of H^+ , Li^+ and Cs^+ , the ZnPO-X transformed to hopeite ($\text{Zn}_2(\text{PO}_4)_3$), the zincophosphate analog of LiA(BW) and CsZnPO_4 , respectively. The broadening of the symmetric C–N stretching band ($\sim 766 \text{ cm}^{-1}$) of tetramethylammonium trapped in the sodalite cages of ZnPO-X was found to be a marker for the framework distortions. Ion-exchange led to distortions of the framework and promoted the hydrolytic instability of the ZnPO-X framework. It is being proposed that in the case of H^+ exchange, protons penetrate into the structure and dissolution occurs by solubilization of the topmost layers of the crystal which leads to a local supersaturated state that results in nucleation of hopeite. Growth of hopeite occurs via nutrients available from dissolution of succeeding layers of the ZnPO-X. For the Li^+ and Cs^+ , considering the neutral pH during exchange, proton penetration into the framework should be negligible. Dissolution then must begin at the outermost crystal surface and the solubilized zinc and phosphate ions combine with the cations in solution to form LiA(BW) and CsZnPO_4 . © 2001 Elsevier Science B.V. All rights reserved.

Keywords: Zincophosphate-X; Dissolution; Raman microprobe spectroscopy

1. Introduction

Dissolution of microporous materials, though an important issue in the area of microporous materials science, has not been studied as extensively as the formation of these materials. Many microporous materials, especially the open framework types, are metastable structures and evolve to more stable, condensed structures via dissolu-

tion [1]. Partial dissolution of zeolites is an important process used to generate catalytically active dealuminated zeolites [2]. Most of the literature on dissolution relates to microporous aluminosilicates, including transformation to different frameworks, the role of co-cations in the process as well as dissolution to soluble species [3]. Traditional methodologies for studying crystal dissolution/transformation involve analysis via diffraction techniques or elemental analysis of soluble species. Zeolite dissolution in highly basic solutions has been studied. For low Si/Al ratio zeolites, such as zeolite A, X, mordenite [4–6], the

* Corresponding author. Tel.: +1-614-292-4532; fax: +1-614-292-1685.

E-mail address: dutta.1@osu.edu (P.K. Dutta).

dissolution took place in accordance to the model of Davies and Jones [7], which predict the presence of a monolayer of solvated ions with constant composition at the dissolving crystal surface. For high Si/Al zeolites, such as ZSM-5, the dissolution process was incongruent, a layer of amorphous SiO₂ was found on the ZSM-5 and the ability of the structure directing tetrapropylammonium cation to form soluble silicate complexes influenced the dissolution process [8]. An interferometric technique for dissolution of ZSM-5 noted that dissolution is dependent on the chemical (especially Al content) and geometrical characteristics of the crystal [9]. For completely siliceous zeolite, silicalite, the activation energies for dissolution of three crystal faces was found to be comparable and similar to that of quartz. The structure of the dissolving unit was not determined [10]. Electron microscopy of the surface has also provided insight of morphological changes during crystal dissolution [11]. In situ analysis of the transformation process, especially with the aid of spectroscopic probes that provide structural information is scarce. More recently, with the development of scanning probe microscopies, it has become possible to examine atomic level changes on the crystal surface after dissolution [12].

In this paper, we focus on an in situ vibrational spectroscopic study of dissolution of zincophosphate crystals with the faujasite topology. Stucky and coworkers have reported a series of zincophosphates that have structures analogous to zeolites e.g. faujasitic and sodalite topologies [13,14]. A major advantage of working with these frameworks is that their synthesis and dissolution can be done under ambient conditions. We have exploited the mild synthesis conditions to make zincophosphates from reverse micelles [15–19]. In addition, in a recent study we have shown that by altering the reaction composition, the morphology of faujasitic zincophosphate X (ZnPO-X) can be altered from conventional ~10 μm octahedral crystals to flat crystals of ~100 μm dimensions [20]. The availability of the platelet crystals led us to examine the crystal dissolution of single crystallites by microprobe Raman spectroscopy and has provided information about the role of co-cations in

the dissolution/transformation of ZnPO-X and forms the subject matter of this paper.

2. Experimental section

2.1. Reagents and methods

Concentrated hydrochloric acid (37.2%), sodium chloride (99%), potassium bromide (IR grade) and sodium hydroxide pellets (98%) were obtained from Fisher, lithium chloride (99.8%) and sodium citrate (99.8%) from Mallinkrodt, cesium chloride (99.9%), tetramethylammonium bromide (TMABr, 98%) from Aldrich, sodium nitrate (99%) from J.T. Baker and sodium bromide (>99%) from MCB Reagents. A 5% ethanolic solution of bromocresol green was used as a marker dye.

ZnPO-X platelets were synthesized following the procedure described in the Ref. [20]. Acid buffer solutions were prepared by combining sodium citrate, sodium chloride and sodium hydroxide or hydrochloric acid in different ratios according to the Fluka catalog. A (Na, TMA)-containing pH 10 buffer was prepared by adding enough TMABr and sodium chloride to a Fisher Certified Buffer Solution pH 10.00 (composed of potassium carbonate, potassium hydroxide) making a solution 0.20 and 1.0 M in Na⁺ and TMA⁺, respectively. ZnPO-X crystals were ion-exchanged with LiCl (0.1 and 1.0 M), NaBr (1.0 M), KBr (1.0 M), and CsCl (1.0 M) in separate experiments. After ion-exchange, the samples were also analyzed by X-ray powder diffraction.

2.2. Instrumentation

Raman spectra were obtained in a Dilor XY modular spectrometer in the 500–1500 cm⁻¹ range using Argon ion laser excitation (excitation at 514 nm). The instrument is attached to an Olympus microscope and to a video camera. A 40× magnification immersion lens was used. Powder X-ray diffraction (XRD, Rigaku Geigerflex D/max-2B) patterns were recorded using CuK_α radiation. The samples were analyzed between 2° and 50° 2θ (in step mode with a fixed time of 3 s per scan and a

scanning interval of 0.04°). Scanning electron micrographs were taken on a JEOL JSM-820 instrument. The samples were coated with Au–Pt mixture to avoid charging the sample.

3. Results

Fig. 1(left) shows a SEM micrograph of octahedral ZnPO-X crystals, the normal habit assumed by these crystals [13]. However, by increasing the $\text{Zn}^{2+}/\text{Na}^+$ ratio from 1.5 to 2.1, TMAOH/ H_3PO_4 from 2.09 to 2.44 and dilution of the system by 30% [20], the morphology can be converted to platelike crystals, (Fig. 1, right). This change in morphology originates from a single twin plane bisecting the hexagonal platelets edgewise and can be readily observed on the edges of the crystal in Fig. 1. These flat platelet crystals, both because of their large size ($\sim 100\ \mu\text{m}$) and flatness are well suited for Raman microscopy experiments, in which a laser spot is focused on the flat face of the crystal. By using an objective lens that can be immersed into the solution, in situ studies of the crystal transformation were carried out.

3.1. Influence of cations on the transformation of ZnPO-X

The transformation of ZnPO-X in the presence of several monovalent cations in solution was ex-

amined, including Li^+ , Na^+ , K^+ , Cs^+ , and H^+ . Structural changes resulting in alteration of the ZnPO-X framework were noted by X-ray diffraction only in the Li^+ , Cs^+ and H^+ systems and the spectroscopic measurements were carried out on these three systems.

3.1.1. Protons

The effect of putting ZnPO-X crystals into a buffer of $\text{pH} \sim 3$ was followed by optical microscopy. Fig. 2 shows the optical micrographs as a function of time. During the first 10 min, no change in size of the crystal was observed, and the morphology was conserved except for rounding of the edges. Fig. 2a shows the crystal after 10 min. Then, over the next 10 min, the crystal was found to decrease rapidly in size, (Fig. 2b, 20 min) and finally after 22 min, the crystal has completely dissolved (Fig. 2c). The local pH around a ZnPO-X crystal also changed with dissolution. This was evident by adding the dye bromocresol green to the ZnPO-X crystals maintained at $\text{pH} \sim 3$. At this pH, bromocresol green is a yellow color. However, with the initiation of dissolution, in the vicinity of the ZnPO-X crystals, the color of the dye turned green, indicating that the solution around the dissolving crystal became more basic.

Fig. 3 shows the microprobe Raman spectra obtained from the surface of a ZnPO-X, as a function of exposure time to a pH 3 solution. The initial bands at 766 , 958 and $1454\ \text{cm}^{-1}$ are due to

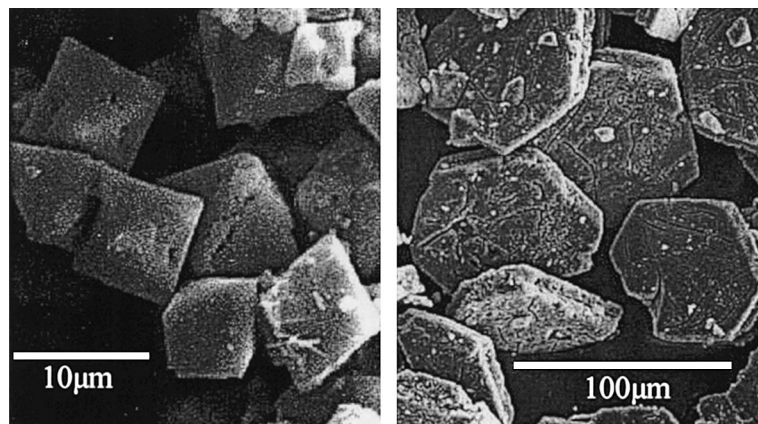


Fig. 1. SEM micrographs of ZnPO-X crystals demonstrating the change in morphology from conventional octahedral crystals (left) to platelet crystals (right).

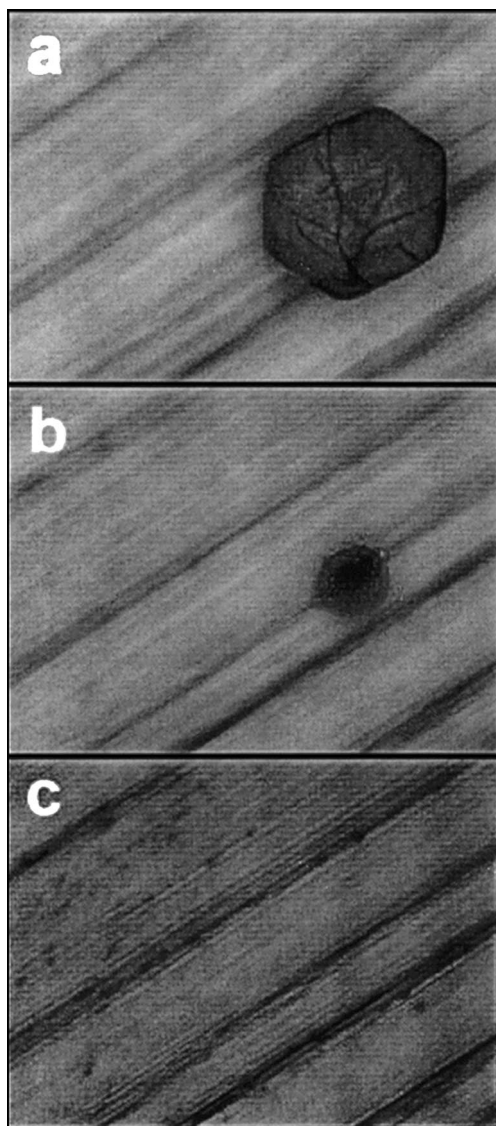


Fig. 2. Optical micrograph showing dissolution of a ZnPO-X crystal at pH 3 as a function of time (a) 10 min (b) 20 min (c) 22 min.

the TMA ions entrapped in the sodalite cages of ZnPO-X and the bands at 983, 1010, 1096 and 1123 cm^{-1} are due to the ZnPO-X framework [17]. Because of the shift in the frequencies of TMA upon encapsulation (especially the C–N stretching mode from 754 to 766 cm^{-1}) [21], it is relatively easy to distinguish free and bound TMA. Within the first 4 min of contact with the acidic solution, a

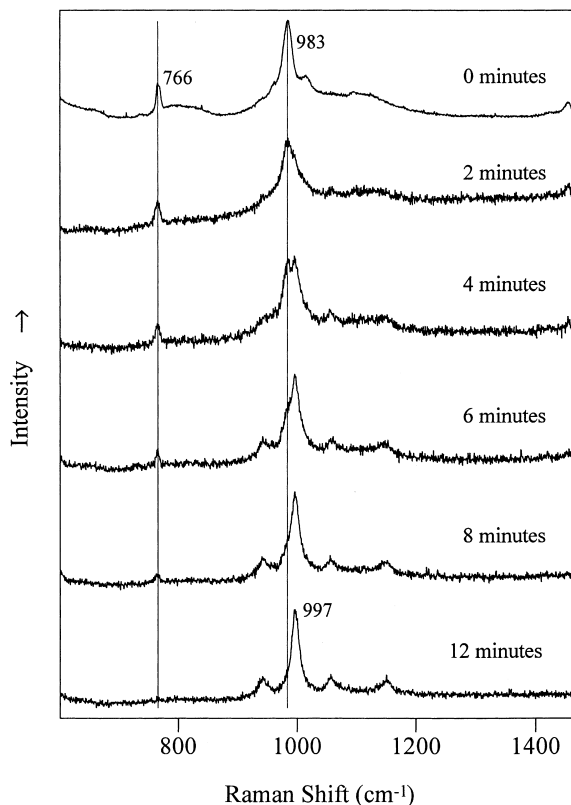


Fig. 3. Microprobe Raman spectra of a dissolving ZnPO-X crystal at pH 3 as a function of time.

broadening of the 766 cm^{-1} band from 6 to 11 cm^{-1} was noted, and there is also the appearance of a set of new bands at 944, 997, 1058 and 1150 cm^{-1} , which is assigned to hopeite, $\text{Zn}_3(\text{PO}_4)_2$ based on the diffraction patterns, as we discuss below. The optical microscopy indicates that the crystal morphology has remained unaltered. Within a period of 12 min, the bands due to TMA present in the ZnPO-X have completely disappeared along with the ZnPO-X framework bands and are replaced by the new bands. The rate of disappearance of the entrapped TMA bands and ZnPO-X framework bands was similar to the appearance of the new Raman bands. Bands due to free TMA in solution were not observed.

Electron microscopy of the crystals recovered from the acid treated samples at various times is shown in Fig. 4. Before acid treatment, the characteristic hexagonal platelets are observed (Fig. 4a).

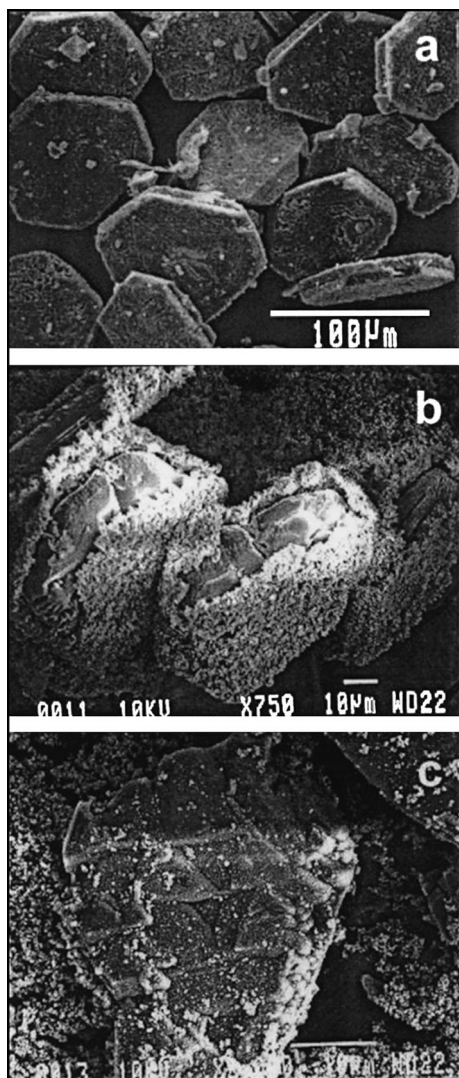


Fig. 4. SEM micrographs of ZnPO-X crystals (a) original sample (b) after exposure to pH 3 buffer for 10 min (c) sample in (b) washed with pH 10 buffer.

After 10 min, the crystals are coated with a solid (Fig. 4b), and the original crystal can be seen through a rupture in the coating. The coating can be removed by treatment with base (pH 10, Fig. 4c), rendering a surface that has a Raman spectrum and diffraction pattern of ZnPO-X. The surface of the partially dissolved ZnPO-X is rough and made up of triangular motifs. Fig. 5a shows a closer view of the SEM micrograph of the solid material that is formed on the ZnPO-X surface

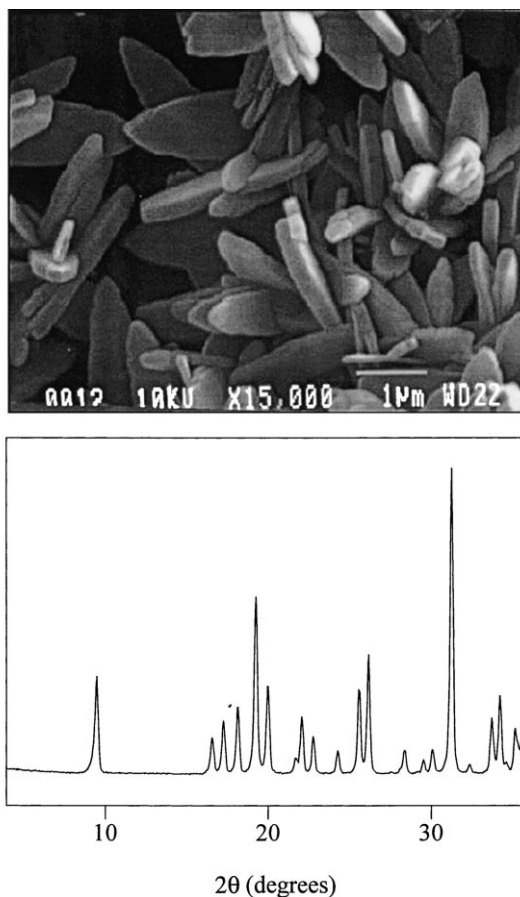


Fig. 5. (a) SEM micrograph and (b) powder diffraction pattern of the coating on the ZnPO-X crystal formed after exposure to pH 3 buffer for 10 min.

and Fig. 5b its powder diffraction pattern. This pattern can readily be identified to be that of hopeite, $Zn_3(PO_4)_2$ [14] and the solid also has a Raman spectrum with bands at 944, 997, 1058 and 1150 cm^{-1} .

3.1.2. Lithium ions

For the Li^+ and Cs^+ exchanged samples, the Raman spectra were obtained after ion-exchange. With a 0.1 M Li^+ solution, the Raman spectrum of ZnPO-X exhibits two major changes as compared to the Na^+ form (Fig. 6a). The symmetric stretching band of the sodalite encapsulated TMA at 766 cm^{-1} shifts to 772 cm^{-1} along with a broadening of the peak and the strongest framework band of

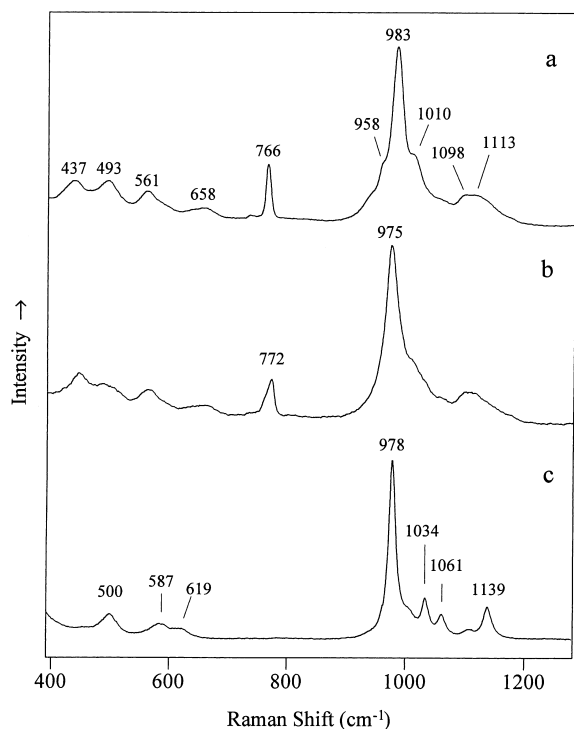


Fig. 6. Raman spectrum of (a) ZnPO-X (b) after ion-exchange with 0.1 M LiCl (c) exposed to 1 M LiCl for several days.

ZnPO-X shifts from 983 to 975 cm^{-1} . These changes in the vibrational spectrum took place within minutes of exchange and could be reversed by ion-exchange with Na^+ . In the presence of 1 M LiCl for an extended period of time (several days), the Raman spectrum was irreversibly changed as shown in Fig. 6c. Powder diffraction pattern showed that the ZnPO-X had transformed to the zincophosphate analog of LiA(BW).

3.1.3. Cesium ions

In the presence of 1 M CsCl, the initial change that is noted is a broadening of the C–N symmetric stretching at 766 cm^{-1} , as compared in Fig. 7a and b. However, within 60 h, the remaining solid showed no presence of TMA^+ and the framework bands are different from ZnPO-X, (Fig. 7c). Powder diffraction data show that the ZnPO-X has transformed to mainly monoclinic CsZnPO_4 (powder diffraction file JCPDS 45-277).

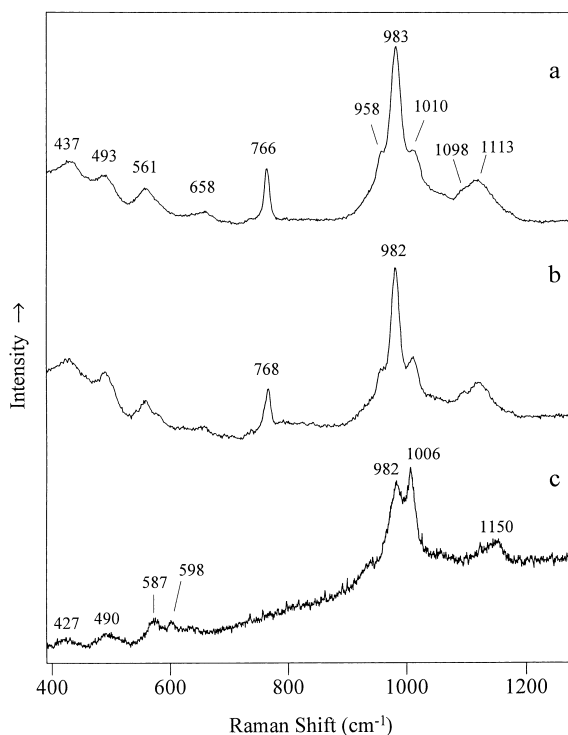


Fig. 7. Raman spectrum of (a) ZnPO-X (b) after 2 h exchange with 1 M CsCl (c) after 60 h exchange with 1 M CsCl.

4. Discussion

The transformation of octahedral to hexagonal platelet crystals is controlled by the reactant composition, and results from a twin plane. There have been patent reports in the literature on synthesis of platelet faujasite-type crystallites, via introduction of twin faults [22], and require the presence of K^+ and Cs^+ . The formation of ZnPO-X platelet crystals required the decrease of Na^+ relative to that of Zn^{2+} , and we have proposed that the excess Zn^{2+} ions are favoring the twinning process [20].

In the presence of all three cations, H^+ , Li^+ and Cs^+ , the ZnPO-X is unstable in the time frame of hours per days and transforms to hopeite, LiA(BW) and CsZnPO_4 , respectively. However, ZnPO-X was stable in 1 M Na^+ solutions for months.

A correlation was noted between the band broadening of the band at 766 cm^{-1} due to sodalite-entrapped TMA and ion-exchange with the

various cations. This band is assigned to the symmetric C–N stretch of the TMA molecule, and appears at 754 cm^{-1} in solution. The increase in the symmetric stretching frequency upon encapsulation arises because the size of the TMA molecule is very close to the internal volume of a sodalite cage which offers resistance to the increase in volume required for the symmetric stretch [21]. The data presented in Fig. 8 shows that the bandwidths for the 766 cm^{-1} band upon ion-exchange with Na^+ , H^+ , Cs^+ , and Li^+ follow the order 6, 11, 12 and 17 cm^{-1} . In the case of Li^+ , which exhibits the most broadening, there is also a shift of the strongest zincophosphate framework band from 983 to 975 cm^{-1} , and these changes are reversible upon ion-exchange back with Na^+ , indicating that it must be occurring from distortion in the framework. Framework distortions brought about by ion-exchange have been reported in the Ref. [23]. Vibrational spectroscopic data of the framework of several zeolites has been shown to vary with cation exchange [24,25]. We propose that the electrostatic interactions of the cations with the framework alters the T–O–T angles and creates a distribution of environments for the TMA entrapped in the sodalite cages that lead to the band broadening. The framework distortions are manifested in the C–N stretching frequency

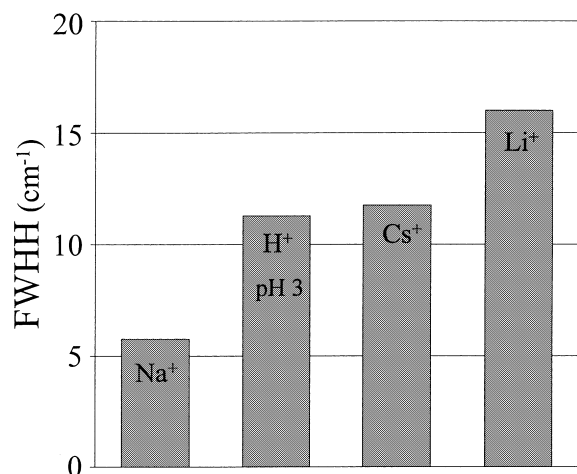


Fig. 8. Comparison of the broadening of the symmetric stretch of the sodalite entrapped tetramethylammonium ion band at $\sim 766\text{ cm}^{-1}$ in the presence of various co-exchanged cations.

because of the tight fit of TMA into the sodalite cage [21].

Optical microscopy of a dissolving platelet of ZnPO-X shows that the initial morphology is maintained for a period of ~ 10 min, followed by gradual loss of the shape, as evidenced by its diminishing size. Both electron microscopy and Raman spectroscopy clearly demonstrate that within the first 10 min, a layer of hopeite is forming around the dissolving ZnPO-X crystal. The experiments with the bromocresol green indicator shows that there is a local increase in pH around the dissolving crystallite. We propose that the following reaction is involved in the overall dissolution.



The experiment with bromocresol green was repeated with pure hopeite crystals in a buffered solution of $\text{pH} \sim 3$, but no color change was noted around the dissolving crystal, suggesting minimal pH changes. On a microscopic level, the dissolution can be viewed as a process in which ZnPO-X, via some intermediate species dissolves to eventually form Zn^{2+} and PO_4^{3-} ions. The solubility product of $\text{Zn}_3(\text{PO}_4)_2$ is of the order of 10^{-35} , thus even with mass transport of Zn^{2+} and PO_4^{3-} ions away from the dissolving crystal, supersaturation conditions for crystallization of hopeite are being exceeded. The precipitation of $\text{Zn}_3(\text{PO}_4)_2$ leaves behind an excess of PO_4^{3-} , which can combine with H^+ raising the pH around the dissolving crystal. Eventually the hopeite also dissolves, as is evident from Fig. 2. If the dissolution of ZnPO-X is carried out at $\text{pH} \sim 3$ with agitation of the solution, then Raman microscopy does not show the presence of hopeite. With facilitated mass transport, the Zn^{2+} and PO_4^{3-} ions do not have the opportunity to exceed supersaturation.

AFM on zeolite Y with the same topology as ZnPO-X suggest that the (1 1 1) face growth occurs in a layer-by-layer manner, resulting in terraces separated by steps [26]. A similar surface structure can be expected for ZnPO-X. Dissolution of heulandite, a natural zeolite has been studied in acidic and basic solutions by AFM [12]. It was found that dissolution occurred by loss of aluminosilicate

species from terraces in a layer-by-layer fashion. Extensive formation of pits on the terraces were noted and explained via penetration of H^+/OH^- through the micropores and subsequent hydrolysis of T–O–T bonds connecting the layers. In the present case, the Raman microscopy samples a depth of $\sim 1 \mu\text{m}$, which is of the order of ~ 1000 layers. The spectroscopic changes, including the broadening of the TMA band occurs within minutes of exposure to H^+ , indicating that the H^+ penetration deep into the crystal occurs rapidly. We notice that over this depth of ~ 1000 layers, there is a gradual decrease in ZnPO-X and increase in formation of hopeite with time. No intermediate species were observed. This implies that gradual dissolution of the zincophosphate occurs, with immediate formation of hopeite from the dissolution products of ZnPO-X. These observations are consistent with the layer-by-layer-dissolution model proposed for heulandite [12].

Another model of dissolution would involve formation of an amorphous phase followed by dissolution. Such an observation was made by Cook et al. for dissolution of zeolite A ($\text{Na}_{12}(\text{AlO}_2 \cdot \text{SiO}_2)_{12}$) at various pH values (pH 3–9) [27]. They also noted the two roles of the protons: ion-exchange and hydrolysis, with the initial ion-exchange process being reversible. Also, the morphology was maintained in the presence of acid between pH 5–7 though the zeolite had completely lost its structure by hydrolysis and became amorphous with a more dense structure. We can definitely exclude this dissolution pathway, since no amorphous state was observed. Also, the fact that disturbance of the solution around the dissolving crystal via stirring does not lead to the formation of hopeite suggests that the local supersaturation condition can be readily destroyed implying that the amount of material is being dissolved is small consistent with a layer-by-layer dissolution.

Dissolution of zeolite A was found to be incongruent, with the silicon being preferentially dissolved, leaving an aluminum enriched surface [27]. Similar conclusions were reached with heulandite, where dissolution was proposed to occur via loss of Al species, leaving behind a siliceous interface [28]. The spectroscopic data showing that ZnPO-X is maintained even after partial dissolu-

tion to hopeite, as well as the pH change noticed around the dissolving crystal indicates that dissolution of ZnPO-X occurs in a congruent fashion.

ZnPO-X appears to be indefinitely stable in Na^+ exchanged form, but disintegrates in the presence of Li^+ and Cs^+ at neutral pH. As we have noted above, the Li^+ and Cs^+ exchanged ZnPO-X appears to have its framework distorted relative to that of the Na^+ form. We propose that these distortions make the Zn–O–P bond more susceptible to hydrolysis. Because of the high local concentrations of Li^+ and Cs^+ , the dissolved Zn^{2+} and PO_4^{3-} species react to form LiA(BW) and CsZnPO_4 , respectively. In the case of acidic solutions, there are two effects. Structural distortions occur upon ion-exchange of H^+ into the framework making it more susceptible to hydrolysis, and the protonation of the Zn–O–P bonds promote the rapid dissolution of the framework and the formation of hopeite. In the case of a natrolite–thomsonite intergrowths, it was noted that with K^+ in the medium, the framework was stabilized towards acidic media, presumably because K^+ kept the H^+ from exchanging into the framework [29]. This would explain the slow dissolution process we observe in the Li^+ and Cs^+ system, even though the framework distortions are significant. In these cases, the dissolution would have to occur beginning with attack by the protons on the exterior part of the framework, since the process is occurring in the presence of considerable excess of the alkali-metal ions, and replacement of the alkali-metal ions in the crystal by protons is unlikely. Mechanisms of proton-induced dissolution of aluminosilicates have been proposed to be initiated by detachment of aluminum species by hydrolysis of Al–O–Si bond [28]. Even though, the hypothesis of initiation of hydrolysis via the Al–O–Si bond is reasonable, it is unknown if dissolution occurs by loss of monomeric or oligomeric species and how this is influenced by the framework structure.

5. Conclusions

Dissolution of large platelet-like crystals of faujasitic ZnPO-X was studied by microprobe Raman spectroscopy in the presence of a series of

monovalent ions. In the presence of H^+ , Li^+ and Cs^+ , hopeite, the zincophosphate analog of LiA (BW) and $CsZnPO_4$ were formed, respectively. Upon exchange of these three cations, the framework of $ZnPO-X$ was distorted to different degrees and monitored by the band broadening of the C–N symmetric stretch of the sodalite-entrapped TMA ion. The strongest structural distortions were in the case of Li^+ and could be reversed by Na^+ exchange. These framework distortions made the structure more susceptible to hydrolysis and brought upon the destruction of the $ZnPO-X$ framework. In the case of H^+ exchange, the $ZnPO-X$ dissolution resulted in formation of a hopeite ($Zn_2(PO_4)_3$) coating on the crystal. Compared to H^+ ion-exchange, the hydrolysis reaction promoted by protons is slower and does not proceed through formation of an intermediate amorphous phase. It is proposed that transformation occurs in a congruent fashion via dissolution of the top layers to produce a supersaturated solution, which nucleates hopeite. Gradual dissolution of successive layers supplies the nutrients for hopeite growth.

Acknowledgement

We acknowledge funding from NASA for this research.

References

- [1] D.W. Breck, *Zeolite Molecular Sieves*, Wiley, New York, 1974.
- [2] Y. Chen, *ACS Symp. Series* 738 (2000) 322.
- [3] R.M. Barrer, *Hydrothermal Chemistry of Zeolites*, Academic Press, London, 1982.
- [4] A. Cizmek, L. Komunjer, B. Subotic, M. Siroki, S. Roncevic, *Zeolites* 12 (1992) 190–196.
- [5] A. Cizmek, L. Komunjer, B. Subotic, M. Siroki, S. Roncevic, *Zeolites* 11 (1991) 258–264.
- [6] A. Cizmek, L. Komunjer, B. Subotic, M. Siroki, S. Roncevic, *Zeolites* 11 (1991) 810–815.
- [7] C.W. Davies, A.L. Jones, *Trans. Faraday Soc.* 51 (1955) 812.
- [8] A. Cizmek, B. Subotic, I. Smit, A. Tonejc, R. Aiello, F. Crea, A. Nastro, *Micropor. Mater.* 8 (1997) 159–169.
- [9] T. Sano, Y. Nakajima, Z.B. Wang, Y. Kawakami, K. Soga, A. Iwasaki, *Micropor. Mater.* 12 (1997) 71–77.
- [10] A. Iwasaki, T. Sano, *Zeolites* 19 (1997) 41–46.
- [11] V. Alfredson, T. Oshuna, O. Terasaki, J.O. Borin, *Angew. Chem. Int. Ed. Engl.* 32 (1993) 1210.
- [12] S. Yamamoto, S. Sugiyama, O. Matsuoka, K. Kohmura, T. Honda, Y. Banno, H. Nozoye, *J. Phys. Chem.* 100 (1996) 18474–18482.
- [13] T.M. Nenoff, W.T.A. Harrison, T.E. Gier, G.D. Stucky, *J. Am. Chem. Soc.* 113 (1991) 378.
- [14] T.E. Gier, T.A. Harrison, T.A. Nennof, G.D. Stucky, *Molecular Sieves*, in: M.L. Occelli, H. Robson (Eds.), Van Nostrand, Reinhold, NY, 1992, p. 407.
- [15] P.K. Dutta, K.S.N. Reddy, L. Salvati, M. Jakupca, *Nature* 374 (1995) 44.
- [16] K.S.N. Reddy, L.M. Salvati, P.K. Dutta, P.E. Abel, K.L. Suh, R.R. Ansari, *J. Phys. Chem.* 100 (1996) 9870.
- [17] M.J. Castagnola, P.K. Dutta, *Micropor. Mater.* 20 (1998) 149.
- [18] M.J. Castagnola, P.K. Dutta, *Micropor. Mater.* 34 (2000) 61.
- [19] R. Singh, P.K. Dutta, *Langmuir* 16 (2000) 4148.
- [20] M.J. Castagnola, P.K. Dutta, *Proceedings of the 12th International Zeolite Conference*, in: M.M.J. Treacy, B.K. Marcus, M.E. Bisher, J.B. Higgins, (Eds.), MRS, Pennsylvania, vol. 3, 1998, pp. 1627–1632.
- [21] P.K. Dutta, B. Barco, D.C. Shieh, *Chem. Phys. Lett.* 127 (1986) 200.
- [22] D.E.W. Vaughan, M.G. Barret, *US Patent* 333 (4) (1982) 859.
- [23] T. Bauer, W.H. Baur, *Eur. J. Mineral.* 10 (1998) 133.
- [24] P.K. Dutta, B. Delbarco, *J. Phys. Chem.* 89 (1985) 1861.
- [25] Z. Sobalik, Z. Tvaruzkova, B. Wichterlova, *J. Phys. Chem. B.* 102 (1998) 1077.
- [26] M. Anderson, J. Agger, J. Thornton, N. Forsyth, *Angew. Chem. Int. Ed. Engl.* 35 (1996) 1210–1213.
- [27] T. Cook, W. Cilley, A. Savitsky, B. Wiers, *Environ. Sci. Technol.* 16 (1982) 344–350.
- [28] K.V. Ragnarsdottir, C.M. Graham, G.C. Allen, *Chem. Geol.* 131 (1996) 167–181.
- [29] D. Charistos, A. Godelitsas, C. Tsipis, M. Sofoniou, J. Dwyer, G. Manos, *Appl. Geochem.* 12 (1997) 693–703.